CONFERENCE PRE-PRINT

COMPATIBILITY OF PRONOUNCED DETACHMENT WITH IMPROVED CONFINEMENT ON HL-2A TOKAMAK

Ting Wul, Min Xul, Zhuo Wangl, Lin Niel, *, Zhanhui Wangl, Jinming Gaol, Yihang Chenl, Yiren Zhul, Yi Zhangl, Liang Liul, Dong Lil, Kai Zhangl, Rui Kel, Xiaoxue Hel, Zengceng Yangl, Xin Yul, Na Wul, Zhihui Huangl, Kaiyang Yil, Weice Wangl, Longwen Yanl, Yonggao Lil, Ting Longl, Wenjing Tianl, Zhe Wangl, Laizhong Cail, Yi Yu2, *

1Southwestern Institute of Physics, Chengdu 610041, China 2Sino-French Institute of Nuclear Engineering and Technology, Sun Yat-sen University, Zhuhai 519082, China

Email: wuting@swip.ac.cn

Abstract

This paper investigates the compatibility of pronounced detachment with improved confinement based on the NBI-heated HL-2A L-mode plasma with low-density. Through impurity seeding, radiation becomes higher at plasma edge and causes edge cooling after pronounced detachment. Turbulent transport is examined in detail by experiments and global integrated simulations. Ion dominant turbulent transport decreases at normalized minor radius $\rho \in [0.1, 0.4]$ and ion temperature increases at $\rho \in [0.0.8]$. Edge turbulence and turbulent transport through ion channels decrease significantly, which could result from reduced free energy source due to edge cooling. The reduced edge turbulent transport benefits to decrease the power entering the SOL/divertor. The decreased edge outward transport and increased core electron density and ion temperature make major contributions to the improved plasma confinement after pronounced detachment.

1. INTRODUCTION

Heat load control on the divertor target is a critical issue for International Thermonuclear Experimental Reactor (ITER) and future fusion reactors. The detachment scenario is a promising way to achieve steady state H-mode plasma in ITER [1,2]. However, divertor detachment sometimes leads to degraded core confinement [3-10]. Especially in the pronounced and full detached states [4], excessive impurity accumulation in the main plasma causes confinement degradation [3-4, 11-12]. Hence, various feedback methods of controlling impurities are employed to avoid excessive impurity injection, so as to improve the compatibility of detachment with core confinement after detachment [13-28]. For example, injecting appropriate amounts of impurity gas through feedback to control the location of the X-point radiator (XPR) [13-17] outside the X-point can reduce confinement degradation. In addition, the closed divertor configuration has special advantages to achieve divertor detachment [7, 18-26]. Closed divertor facilitates detachment at relatively low density [7, 18-23], and benefits impurity screening [24-26]. Plasma performance is better after detachment with closed divertor configuration compared to that with open divertor configuration [7, 18-21]. Moreover, good compatibility of actively controlled full divertor detachment with high performance plasma is achieved by a core internal transport barrier (ITB) and a modest edge transport barrier (ETB) increasing confinement in high poloidal beta scenario in DIII-D [18-19]. Studying the compatibility of divertor detachment with core confinement is of great interest in recent years.

Traditionally, the core and edge regions have been studied as isolated regions with different physics, even in L-mode plasmas. In this paper the edge region refers to the region very close to the last closed flux surface (LCFS) and the scrape-off layer (SOL). The core and edge regions have different models in theories and simulations. However, a moment's thought leads to the observation that the edge region is situated immediately adjacent to the core region. The phenomenon that the core and edge regions couple with each other has already been studied in previous literatures [29-32]. In TJ-II stellarator, the edge radial electric field shear is reported to be an important tool for suppressing turbulence and decoupling the regions inside and outside the LCFS [31]. In fact, higher ion temperature in the core region is preferred in order to achieve higher fusion power. Meanwhile, a cooling edge, especially a cooling SOL, provides a beneficial path for controlling the heat loads on the plasma facing components and the divertor target when pursuing high fusion power. Hence, the core and edge regions are required to be decoupled to make high plasma performance and effective divertor power exhaust compatible.

In this paper, then, we explore the core-edge integration solution which can provide higher ion temperature in the core and lower temperature near the LCFS and the strike point in pronounced detached plasma.

In this paper, we present the compatibility of pronounced detachment with improved confinement on HL-2A L-mode plasma. The remainder of this paper is organized as follows. Section 2 describes the experimental setup and section 3 presents improved confinement after pronounced detachment on HL-2A. Section 4 studies the plasma and impurity radiation. The edge turbulence and turbulent transport behaviour are examined experimentally in section 5. An integrated simulation of global electrostatic turbulence is presented in section 6. Section 7 gives a discussion and section 8 presents conclusions and further study.

2. EXPERIMENTAL SETUP

The experiments were conducted on the HL-2A tokamak with lower single null divertor configuration [33]. Here we introduce the divertor configuration and diagnostic systems related to the detachment on HL-2A tokamak. The divertor on HL-2A has a very high degree of closure [24-25]. The minimum distance between baffles and targets at the entrance of the divertor is about 2 cm. The closed divertor configuration has a good screening effect on the neutrals entering the main chamber [24-26]. A gas mixture of nitrogen (60%) and deuterium (40%) is injected from the diverter target into the divertor chamber, and the amount of injected mixture can be controlled by changing the voltage applied to the fast-opening valves. The pumping system includes two turbopumps and two cryopumps. They can pump away the neutrals which have low temperature, and decrease recycling from the divertor chamber wall. There are various diagnostic systems on HL-2A tokamak. Details can be seen in reference [33].

3. IMPROVED CONFINEMENT AFTER PRONOUNCED DETACHMENT ON HL-2A

A typical example of improved confinement after pronounced detachment is shot #38008. During Neutral Beam Injection (NBI) heating, the plasma current is $I_{\rm p}=165$ kA; toroidal magnetic field is $B_{\rm t}=1.3$ T; NBI power is $P_{\rm NBI}=330$ kW; loop voltage is $V_{\rm L}=1.8$ V; line-averaged density is $\overline{n_{\rm e}}=1.5-2.3\times 10^{19}$ m⁻³ with its ratio to Greenwald density limit $\overline{n_{\rm e}}/n_{\rm G}=0.37-0.57$; edge safety factor is $q_{\rm a}=3.1$; the total stored energy is $W_{\rm E}=13-17$ kJ. Detachment on HL-2A L-mode plasma is characterized by decreased $D_{\rm c}$ in the divertor chamber, accompanied by increased line-averaged density and decreased ion saturation current $I_{\rm sat}$ and $T_{\rm e}$ in the inner and outer divertor targets. The closed divertor configuration benefits to make the divertor detached with low line-average density [7, 18-23].

In this paper, when we compare the average values plasma parameters (such as $W_{\rm E}$) in the attached state ($t=1000-1050~{\rm ms}$) and in the pronounced detached state $t=1180-1230~{\rm ms}$, if there is no further explanation. During the time interval $t=1000-1050~{\rm ms}$, the mixture has barely been injected into the divertor chamber. The peak values of $J_{\rm sat}$, $T_{\rm e}$ and q_{\parallel} (average in each time interval) decrease by 80.4%, 74.4% and 95.1%, respectively. The profile of parallel heat flux at $t=1180-1230~{\rm ms}$ is much lower than that at $t=1000-1050~{\rm ms}$. According to the identification of pronounced detachment in reference [4], the time interval $t=1180-1230~{\rm ms}$ (which is longer than the energy confinement time) is recognized to be in the pronounced detached state. It is a short time interval $t=1120-1135~{\rm ms}$ of pronounced detachment in #38008. It lasts for just about 20 milliseconds, which is shorter than the energy confinement time. Plasma is evolving fast and has not reached a relatively stable state, so it is not considered here.

The total stored energy $W_{\rm E}$ increases from 13.9 kJ in the attached state to 16 kJ in the pronounced detached state – increased by a factor of 15%, and energy confinement time $\tau_{\rm E}$ increases from 27 ms to 33.6 ms – increased by 24.4%, as shown in table 1. The $P_{\rm SOL}/R$ ($P_{\rm SOL}$ is the power entering the SOL/divertor and R is the major radius) is 0.23 MW/m in shot #38008. In the pronounced detachment experiments in HL-2A L-mode plasma, $P_{\rm SOL}/R$ is in the range of 0.14 MW/m – 0.7MW/m and $\Delta W_{\rm E}/W_{\rm E}$ is between 2% and 15.1%. This is consistent with the statistical results which show improved confinement after detachment in L-mode plasma on HL-2A [50]. These results show the good compatibility of pronounced detachment with confinement on HL-2A L-mode plasma. The following sections will investigate the physics process of improved confinement after

pronounced detachment elaborately by studying the plasma and impurity radiation and turbulent transport from experiments and simulations.

4. EDGE TURBULENCE AND TURBULENT TRANSPORT BEHAVIOR

This section investigates deeply into edge turbulence and turbulent transport behaviour in attached and pronounced detached states in experiments. We present the results of edge turbulence in the attached and pronounced detached states here. The Langmuir probe arrays measure the poloidal wave number ($k_{\theta} < 3/\text{cm}$) spectrum near the LCFS in both states is shown in figure 1. The edge turbulence propagation in the ion diamagnetic drift direction in the attached state changes to the electron diamagnetic drift direction in the pronounced detached state. By integrating a typical frequency band (20 - 150 kHz) for electrostatic turbulence measured by the Langmuir probe at plasma edge [32], the average values of k_{θ} are 0.58 cm⁻¹ and 0.72 cm⁻¹, and the correlation lengths are 1.1 cm and 0.88 cm in the attached and pronounced detached states, respectively. These results indicate that turbulence propagating in the ion diamagnetic drift direction decreases dramatically, and turbulence propagating in the electron diamagnetic drift direction dominates at the edge; the scale of turbulence structure and the connection length of turbulence become smaller near the LCFS after pronounced detachment.

In addition, DBS can measure the fluctuation intensity near the LCFS in the range $4/\text{cm} < k_\theta < 22/\text{cm}$. Figure 2 shows the time evolution of edge fluctuation intensity in shot #38008, and a comparison of average edge fluctuation intensity in attached and pronounced detached states for 12 shots. In figures 2(a), fluctuation intensity becomes lower in the pronounced detached state. In most shots, the edge fluctuation intensity decreases and the total stored energy increases from attached to pronounced detached states in figure 2(b). This indicates that edge turbulence decreases in pronounced detached state. Both mid-plane Langmuir probe and DBS show consistent results of decreased edge turbulence after pronounced detachment.

We further investigate why edge turbulence and turbulent transport decrease after pronounced detachment. One possible reason of the fuel dilution is not discussed here, since we do not have accurate local measurements of impurities at plasma edge. The major reasons may be the strong suppression by poloidal velocity shear or/and the reduction of free energy source. Both DBS and BES measurements show consistent results that the poloidal velocity decreases sharply and is close to 0 in pronounced detached state. In addition, the poloidal velocity shear measured by BES near the LCFS in the pronounced detached state is smaller than that in the attached state. Thus, it is concluded that the poloidal velocity and its shear are not the major reasons for the reduced edge turbulence and turbulent transport after pronounced detachment.

Secondly, we examine the radial gradients of n_e , T_e , T_i and pressure, from which turbulence obtains free energy. The whole radial profiles of n_e , T_e , T_i , pressure $p = e * n_e (T_e + T_i)$ and its radial gradient $\nabla_r p$ in both states are shown in figures 3 In the pronounced detached state, n_e and T_i increase dramatically in the core region at $\rho \in [0, 0.9]$ and $\rho \in [0, 0.8]$, respectively. The increased n_e and T_i are consistent with the increased pressure and hence the total stored energy. T_e decreases slightly after pronounced detachment. In reference [34], the radial gradients of electron temperature $\nabla_r T_e$ and radial gradients of electron pressure $\nabla_r p_e$ near the LCFS drop to very small magnitudes in the pronounced detached state. n_e , T_e , T_i and p, as well as their radial gradients decrease significantly near the LCFS. These flattened profiles in the pronounced detached state indicate the significantly reduced free energy source for turbulence near the LCFS. Though the edge poloidal flow shear decreases, the reduced free energy source from flattened plasma profiles due to edge cooling after pronounced detachment could be the major reason for the decreased edge turbulence and turbulent transport.

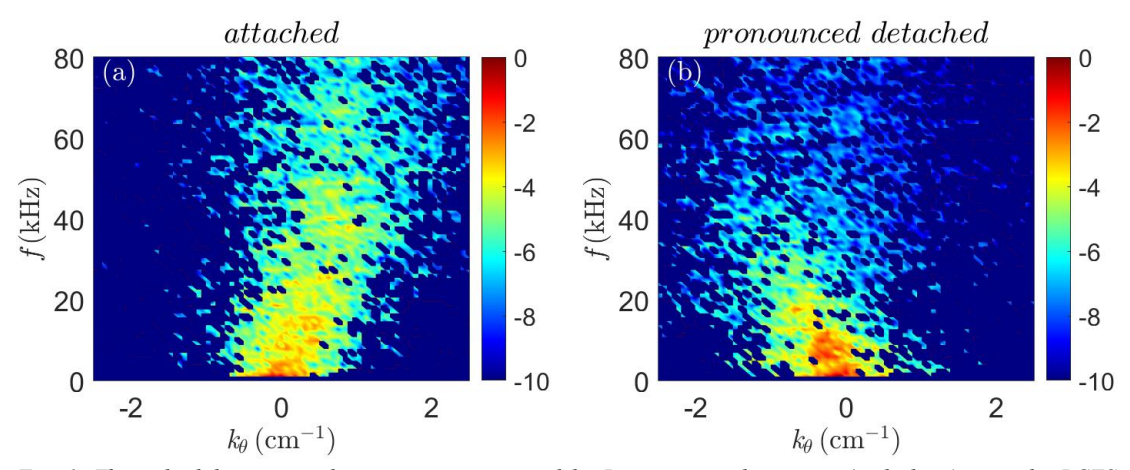


Fig. 1. The poloidal wave number spectrum measured by Langmuir probe arrays (mid-plane) near the LCFS (a) in the attached state and (b) in the pronounced detached state.

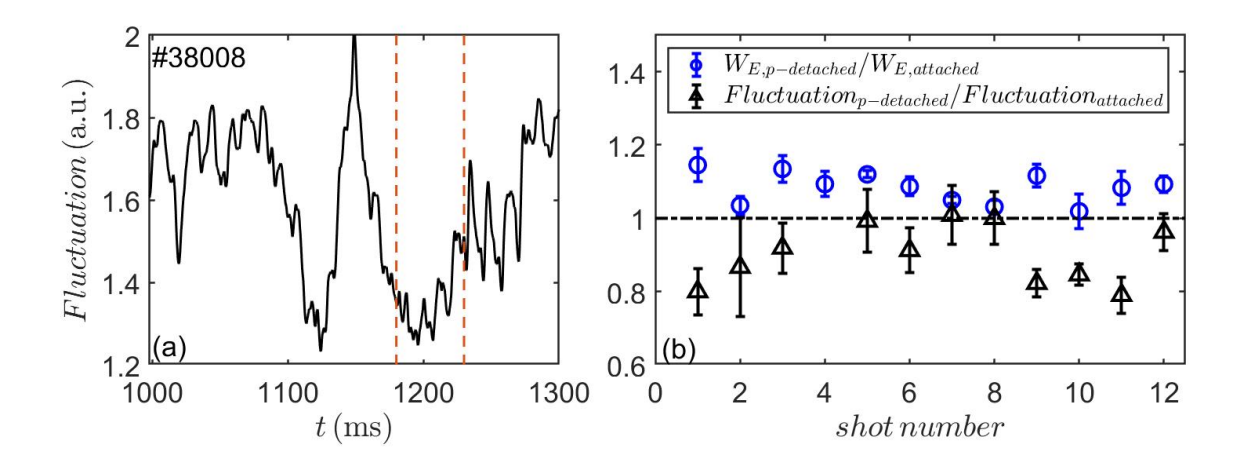


Figure 2. (a) Time evolution of fluctuation intensity measured by DBS near LCFS in shot #38008, and (b) the ratio of total stored energy and average fluctuation intensity (measured by DBS) in pronounced detached state to those in attached states for 12 shots. Here "p-detached" represents the pronounced detached state.

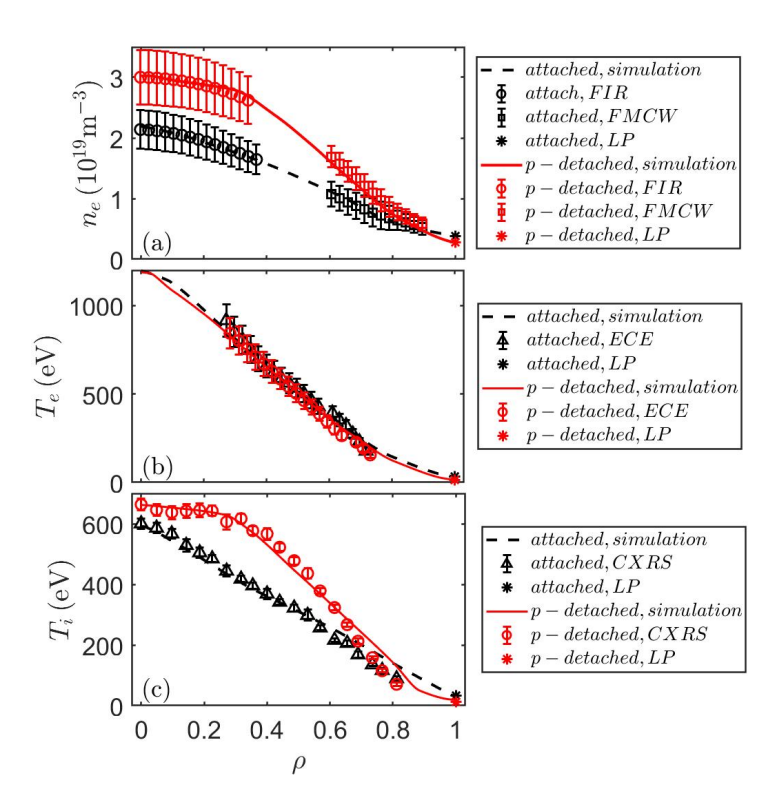


Figure 3. Profiles of (a) electron density n_e , (b) electron temperature T_e and (c) ion temperature T_i in the attached state (t = 1000 ms) and pronounced detached state (t = 1200 ms).

5. INTEGRATED SIMULATION OF GLOBAL ELECTROSTATIC TURBULENT TRANSPORT

An integrated simulation for global electrostatic turbulent transport has been done for the whole cross section, to offset the lack of the experimental measurements in the core region and to complement study at the plasma edge. We consider the electrostatic turbulent transport since it plays a dominant role for L-mode plasma. The integrated simulation is based on the OMFIT platform. We choose one typical time slice in the attached and pronounced detached states, respectively. The initial equilibrium data and plasma profiles (as shown in figure 3) of two typical time slices (t=1000 ms for attachment and t=1200 ms for pronounced detachment) from experiments are employed for the input of simulations, so as to obtain plasma profiles on the whole radius (the solid-lines and dashed-lines in figure 3). In the simulation, the total stored energy is about 12.4 kJ in the attached state and 15.1 kJ in the pronounced detached state. In the experiment, the total stored energy is about 14.3 kJ and 15.6 kJ in both states. The simulation results of total stored energy are qualitatively consistent with the experimental results. So, the plasma profiles from simulation (in figure 3) are used for the input for the global turbulence and turbulent transport analysis in the attached and pronounced detached states in this paper. For L-mode plasma, TGLF-scan is capable to simulate the electrostatic turbulence at $\rho \in [0,0.99]$. We present the simulation results from TGLF-scan as follows.

Firstly, we show the simulation results of the largest growth rate of turbulence in the scale range $k_{\theta}\rho_{s} \in [0,1]$. Here ρ_{s} is the effective ion-sound gyro-radius. Electrostatic turbulence is very weak at $\rho \in [0,0.4]$ in both attached and pronounced detached states. At $\rho = 0.3$, the growth rates of turbulence in the pronounced detached state are lower than that in the attached state. In the attached state, turbulence propagating in the electron diamagnetic drift direction dominates at $\rho \in [0.4,0.9]$, while turbulence propagating in the ion diamagnetic drift direction dominates near the LCFS. In the pronounced detached state, the turbulence propagating in electron diamagnetic drift direction dominates at $\rho \in [0.4,0.99]$. At $\rho = 0.6$, the growth rates of the dominant turbulence in the ion diamagnetic drift direction are similar in both states. At $\rho = 0.8$, the growth rates of

turbulence propagating in the ion diamagnetic drift direction in the pronounced detached state is higher than that in the attached state, which may relate to larger radial gradients of T_i . Near the LCFS, the turbulence propagation direction changes from the ion diamagnetic drift direction to the electron diamagnetic drift direction. More specifically, at ρ =0.99, for relatively large scale $k_{\theta}\rho_s$ \in [0,0.3], the growth rates of turbulence in both ion and electron diamagnetic drift directions in pronounced detached state are much smaller than that of the turbulence in the ion diamagnetic drift direction in attached state; for relatively small scale $k_{\theta}\rho_s$ \in [0.3,1], the growth rates are comparable in both states. The above results suggest that the turbulence propagating in ion diamagnetic drift direction decreases after pronounced detachment near the LCFS. This also agrees with the reduced ∇_r T_i (figure 3) and the change of turbulence propagation direction near the LCFS (figure 1) in the experiments after pronounced detachment. The decreased growth rates of large-scale turbulence in simulation are also consistent with the decreased turbulence scale in experiments after pronounced detachment near the LCFS.

Secondly, we present the simulation results of turbulent particle flux and turbulent energy flux [58] in both states. Normalized turbulent particle flux (Γ/Γ_{GB}) and normalized turbulent energy flux (Q/Q_{GB}) show very similar trends. They are much smaller at $\rho \in [0.1, 0.4]$ in the pronounced detached state than that in the attached state. The dominant ion turbulent energy flux decreases, which may relate to the flattened T_i (figure 3) in this region in the pronounced detachment. Normalized turbulent particle flux and turbulent energy flux are very similar at $\rho \in [0.4, 0.7]$ in both states. They are larger at $\rho \in [0.8, 0.9]$ in the pronounced detached state than that in the attached state, which may be due to larger radial gradients in the profiles in figures 3. At $\rho = 0.99$, Q/Q_{GB} by ions decreases from 305.7 in attachment to 1.5 in pronounced detachment, and Q/Q_{GB} by electrons reduces from 32.6 in attachment to 13.3 in pronounced detachment. The decrement in turbulent transport through ion channels is much larger than that through electrons after pronounced detachment. Combined with the experimental results in figure 1, it suggests that the sharp reduction of turbulent transport through ion channels makes major contributions to the decreased edge turbulent transport.

$6. \quad DISCUSSION-HOW IS PRONOUNCED DETACHMENT COMPATIBLE WITH IMPROVED CONFINEMENT? – AN OVERVIEW$

This paper addresses the compatibility of pronounced detachment with improved confinement on HL-2A. Here we make further study according to power balance in the attached and pronounced detached states. We measure the heating power P_{heat} , total radiation power in the main chamber P_{rad} and the time-variation of the total stored energy dW_{E}/dt from the experiments. The power entering the SOL/divertor P_{SOL} is calculated as $P_{\text{SOL}} = P_{\text{heat}}$ P_{rad} dW_{E}/dt . P_{heat} remains almost unchanged in both states. Here P_{heat} includes NBI power (injected power) and Ohmic heating power. The injected NB power equals nearly to the absorbed power according to NUBEAM simulation. Unfortunately, we are unable to give exact uncertainty of P_{rad} , but its reliability has been estimated statistically in terms of energy conservation. P_{rad} increases from 156 kW to 195 kW while P_{SOL} decreases from 376 kW to 291 kW after pronounced detachment. The decrease in P_{SOL} (85 kW) is larger than the increase in P_{rad} (39 kW). These results indicate that P_{SOL} plays a more significant role than P_{rad} in the time-variation of the total stored energy from attachment to pronounced detachment. The decreased edge turbulent transport contributes to the decreased P_{SOL} .

Here we analyse the possible physical process of the compatibility of pronounced detachment with improved confinement in terms of energy conservation of the plasma reservoir, as summarized in figure 4. The input energy includes heating energy into the main chamber, which remains almost unchanged in the attached and pronounced detached states. The output energy involves the total radiation (plasma radiation and impurity radiation) and outward transport (i.e., $P_{\rm SOL}$). The decrease in the outward transport is larger than the increase in the total radiation, so the output energy reduces after pronounced detachment. Consequently, energy confined in the plasma reservoir increases. Together with the increased $n_{\rm e}$ and $T_{\rm i}$ in the core, total stored energy increases after pronounced detachment.

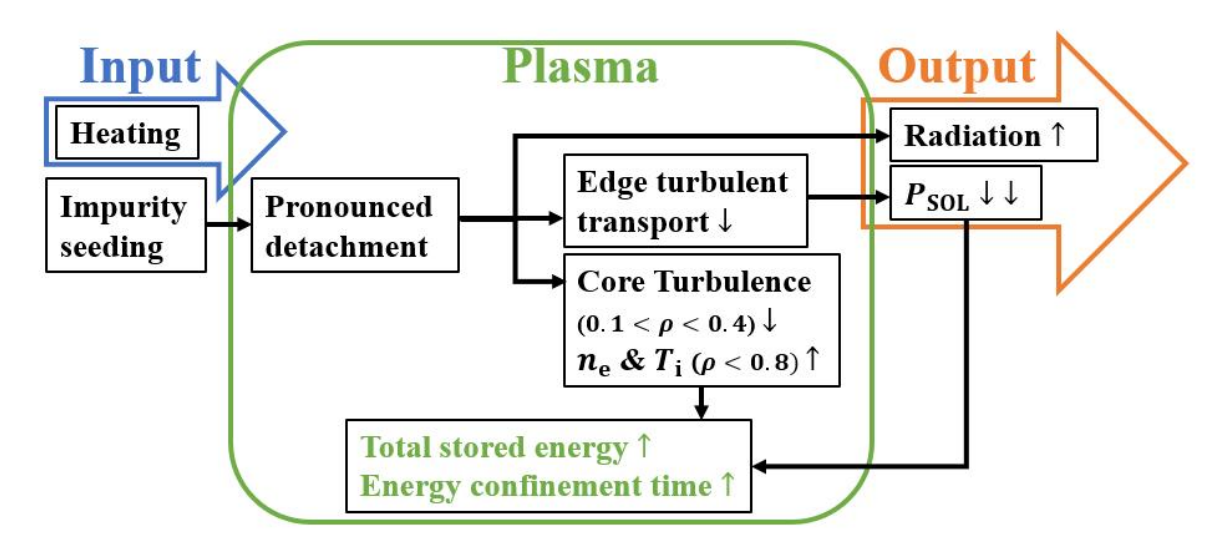


Figure 4. A schematic diagram for understanding the compatibility of pronounced detachment with the improved confinement.

7. REFERENCES

- [1] ITER Physics Basis Editors 1999 Nucl. Fusion 39 2137
- [2] Stangeby P. C. 2000 The Plasma Boundary of Magnetic Fusion Devices (Philadelphia: Institute of Physics Publishing)
- [3] Giroud C. et al 2012 Integration of a radiative divertor for heat load control into JET high triangularity ELMy H-mode plasmas Nucl. Fusion 52 063022
- [4] Kallenbach A. et al 2015 Partial detachment of high power discharges in ASDEX Upgrade Nucl. Fusion 55 053026
- [5] Maddison G. P. et al 2014 Contrasting H-mode behavior with deuterium fueling and nitrogen seeding in the all-carbon and metallic versions of JET Nucl. Fusion 54 073016
- [6] Liu J. B. et al 2019 Divertor detachment and asymmetry in H-mode operation with an ITER-like tungsten divertor in EAST Nucl. Fusion 59 126046
- [7] Wang H. Q. et al 2018 Effects of divertor geometry on H-mode pedestal structure in attached and detached plasmas in the DIII-D tokamak Nucl. Fusion 58 096014
- [8] Li K. D. et al 2020 Divertor detachment with neon seeding in grassy-ELM H-mode in EAST Plasma Phys. Control. Fusion 62 095025
- [9] Li K. D. et al 2021 Comparison of divertor behavior and plasma confinement between argon and neon seeding in EAST Nucl. Fusion 61 066013
- [10] Komm M. et al 2023 Mitigation of divertor Edge Localized Mode power loading by impurity seeding Nucl. Fusion 63 126018
- [11] Covele B. et al 2017 Increased heat dissipation with the X-divertor geometry facilitating detachment onset at lower density in DIII-D Nucl. Fusion 57 086017
- [12] Eldon D. et al 2017 Controlling marginally detached divertor plasmas Nucl. Fusion 57 066039
- [13] Bernert M. et al 2017 Power exhaust by SOL and pedestal radiation at ASDEX Upgrade and JET Nucl. Mater. Energy. 12 111
- [14] Bernert M. et al 2021 X-point radiation, its control and an ELM suppressed radiating regime at the ASDEX Upgrade tokamak Nucl. Fusion 61 024001
- [15] Bernert M. et al 2023 The X-Point radiating regime at ASDEX Upgrade and TCV Nucl. Mater. Energy. 34 101376
- [16] Pan O. et al 2023 SOLPS-ITER simulations of an X-point radiator in the ASDEX Upgrade tokamak Nucl. Fusion 63 016001

- [17] Lunt T. et al 2023 Compact radiative divertor experiments at ASDEX Upgrade and their consequences for a reactor Phys. Rev. Lett. 130 145102
- [18] Wang L. et al 2021 Integration of full divertor detachment with improved core confinement for tokamak fusion plasmas Nat. Commun. 12 1365
- [19] Wang H. Q. et al 2021 Observation of fully detached divertor integrated with improved core confinement for tokamak fusion plasmas Phys. Plasmas 28 052507
- [20] Eldon D. et al 2023 Integration of high confinement, high poloidal beta plasma with dual radiated power and detachment controls for divertor protection and ELM suppression Nucl. Mater. Energy. 34 101332
- [21] Wang H. Q. et al 2023 Study on divertor detachment and pedestal characteristics in the DIII-D upper closed divertor Nucl. Fusion 63 046004
- [22] Sang C. F. et al 2020 SOLPS analysis of changes in the main SOL of DIII-D associated with divertor detachment vs attachment and closure vs openness Nucl. Fusion 60 056011
- [23] Moser A. L. et al 2020 Separating divertor closure effects on divertor detachment and pedestal shape in DIII-D Phys. Plasmas 27 032506
- [24] Gao J. M. et al 2022 Divertor detachment of high βN H-mode discharges with the HL-2A closed divertor geometry Phys. Scr. 97 115604
- [25] Gao J. M. et al 2023 The effect of impurity seeding into the closed divertor on plasma detachment in the HL-2A tokamak Nucl. Fusion 63 036006
- [26] Ma H.C. et al 2023 The behavior and control of injected impurity in the closed divertor of HL-2A Phys. Scr. 98 115608
- [27] Xu G. S. et al 2020 Divertor impurity seeding with a new feedback control scheme for maintaining good core confinement in grassy-ELM H-mode regime with tungsten monoblock divertor in EAST Nucl. Fusion 60 086001
- [28] Li K. D. et al 2023 Compatibility of large ELM control and stable partial detachment with neon/argon seeding in EAST Nucl. Fusion 63 026025
- [29] Fichtmüller M. et al 1998 Core-edge coupling and the effect of the EDGE on overall plasma performance Czechoslovak journal of physics 48 25
- [30] Hahm T. S. et al 2005 On the dynamics of edge-core coupling Phys. Plasmas 12 9
- [31] Grenfell G. et al 2019 Measurement and control of turbulence spreading in the scrape-off layer of TJ-II stellarator Nucl. Fusion 59 016018
- [32] Wu T. et al 2023 How turbulent transport broadens the heat flux width: local SOL production or edge turbulence spreading? Nucl. Fusion 63 126001
- [33] Duan X. R. et al 2022 Progress of HL-2A experiments and HL-2M program Nucl. Fusion 62 042020
- [34] Wu T. et al 2023 Evolution of edge turbulent transport induced by L-mode detachment in the HL-2A tokamak Plasma Sci. Technol. 25 015102

ACKNOWLEDGEMENTS

We are very grateful to Prof. Carlos Hidalgo, Dr. Xiaolan Zou and Dr. Ou Pan for helpful discussions. This work is supported by National Key Research and Development Program of China (Nos. 2022YFE03010004, 2019YFE03030003, 2022YFE03020001, 2022YFE03100004 and 2018YFE0303102), National Natural Science Foundation of China (Nos. 12305235, 12305238, 12305237, 12375210 and U1867222) and the Sichuan Youth Science and Technology Innovation Team Project under Grant No. 2022JDRC0014.